




An experimental approach to reduce precious metal loading on porous transport layer by using magnetron sputtering method for PEMWE application

Anurag, Abhay Gupta, Samaneh Shahgaldi ^{*} 

Hydrogen Research Institute, Université du Québec à Trois-Rivières, Trois-Rivières, G8Z 4M3, Canada

ARTICLE INFO

Keywords:

PEM water electrolyzers
Porous transport layers
Multi-layered coatings
Nb
Pt
galvanic corrosion

ABSTRACT

The extravagant cost of Pt-coated porous transport layers (PTLs) had augmented the already high price of stack components in Proton exchange membrane water electrolyzers (PEMWE). To curtail this high cost, there is a pressing need to replace the expensive Pt coatings with cost-effective materials on Ti PTLs. Hence an attempt is being made to reduce the Pt loading by sputtering co-deposited and multi-layered NbPt coatings on Ti PTLs. The findings showed that the multi-layered NbPt coating exhibited superior corrosion resistance, enhanced durability, and higher conductivity than its co-deposited counterpart under ex-situ environment of PEMWE. The multi-layered NbPt coating was subsequently compared with commercial Pt-coated PTL under both ex-situ and in-situ operating conditions. It was revealed that the multi-layered NbPt coating showcased longer durability and similar ICR compared to the commercial PTL under ex-situ conditions. During the in-situ testing, multi-layered NbPt coating with thin layer of Pt (50 nm), performed (2.050 V @2.0 A/cm²) equivalently to the commercial Pt (200 nm) coating (2.044 V @2.0 A/cm²), making it a viable PTL coating alternative.

1. Introduction

Canada's Net-Zero Emissions Accountability Act, which aligns with the Paris Agreement 2015, set the target for 40–45 % reduction in greenhouse gases (GHG) from 2005 to 2030 and net-zero emission by the year 2050 [1]. To achieve this goal, there is an urgent need to find an alternative to fossil fuels, which accounts for 75 % of GHG and 90 % of CO₂ gas globally [2]. Hydrogen (H₂) fuel, with its high net calorific value (~120 KJ/g), combusts to produce only water as the byproduct, making it a clean and sustainable energy source [3]. However, 96 % of H₂ is produced from the fossil fuels like steam methane reforming and coal gasification process, thereby emitting GHG in the atmosphere [4]. Hence water electrolysis powered by renewable source is the only viable option for producing high purity green H₂. Proton exchange membrane water electrolyzers (PEMWE) produce high purity H₂ with greater efficiency, higher current density and has a quicker response time than Alkaline water electrolyzers [5]. However, the presence of harsh anodic condition, exorbitant cost and insufficient components' durability inhibits the large-scale utilization of PEMWE. One way to reduce production costs is to lower capital expenditure by minimizing the quantity of materials used in PEMWE, while maintaining its performance and durability.

The porous transport layer (PTL), a crucial PEMWE component, not only enables water/gas transport but also electrical and thermal connection between bipolar plate (BPP) and membrane electrode assembly (MEA) [6]. Hence to reduce mass and charge transport losses in PEMWE, which comprises 20–25 % and 20–30 % of total losses, respectively [7], PTL must maintain an equilibrium between its two functions. Previous studies [8,9] have investigated the mechanism related to the evolution and detachment of oxygen (O₂) bubble to reduce mass transport losses. It has been reported [7] that O₂ accumulation inside the PTL leads to membrane dehydration, which affects the oxygen evolution reaction (OER) inside the cell. Next, to account for charge transport losses, PTL must have high electrical conductivity and an efficient electrical contact with MEA and BPP, to reduce interfacial contact resistance (ICR). However, PTL is made of corrosion resistant Ti metal to withstand the harsh anodic conditions inside the cell. The formation of electrically resistive passive film on Ti surface limits its usage unless it is coated with expensive Pt-group metals (PGMs) [10,11]. It has been reported that both Ir-coated [10] and Pt-coated [11] Ti PTLs have lower ohmic resistance than its uncoated counterpart. Moreover, Chang et al. [12] demonstrated that PGMs-coated Ti PTLs prevented catalyst layer delamination by reducing localized hot spots, found in the

^{*} Corresponding author.

E-mail address: samaneh.shahgaldi@uqtr.ca (S. Shahgaldi).

<https://doi.org/10.1016/j.electacta.2025.147053>

Received 24 May 2025; Received in revised form 24 July 2025; Accepted 29 July 2025

Available online 30 July 2025

0013-4686/© 2025 The Authors. Published by Elsevier Ltd. This is an open access article under the CC BY-NC-ND license (<http://creativecommons.org/licenses/by-nc-nd/4.0/>).

case of uncoated PTL.

Owing to their high cost, researchers [13–17] have attempted to fully replace PGMs coatings with cost-effective transition metals-based coatings in both PTLs and BPPs. For instance, Stiber et al. [13] reported that Ti porous sintered layer coating on Ti PTL reduced the ICR by 43 % to 58 $\text{m}\Omega\cdot\text{cm}^2$ @1.5 MPa compared to uncoated counterpart. Conversely, Ye et al. [14] demonstrated that Ta/TaN multi-layered coatings on Ti PTL increased the ICR from 1.58 $\text{m}\Omega\cdot\text{cm}^2$ to 9.71 $\text{m}\Omega\cdot\text{cm}^2$ @1.4 MPa, thereby degrading the PEMWE cell performance. This effect was attributed to increased surface roughness and oxide layer formation in case of Ta/TaN. Likewise, in the separate study, [15] Nb/NbN multi-layered coatings increased the ICR from 15.65 $\text{m}\Omega\cdot\text{cm}^2$ to 31.45 $\text{m}\Omega\cdot\text{cm}^2$ @1.4 MPa, relative to uncoated Ti BPP in PEMWE. These trends were further validated by Meng et al., [16] who reported that 1.6 μm thick Ti, Nb and Ta coated Ti BPPs exhibited higher ICR (331.2 $\text{m}\Omega\cdot\text{cm}^2$, 119.7 $\text{m}\Omega\cdot\text{cm}^2$ and 463.1 $\text{m}\Omega\cdot\text{cm}^2$ @1.5 MPa, respectively) compared to uncoated Ti BPP (36.61 $\text{m}\Omega\cdot\text{cm}^2$ @1.5 MPa) after 24 h of chronoamperometry test at 2.0 V, 80 °C. Although Nb/Ti multi-layered coating on stainless steel (SS) BPP [17] performed equivalently to commercial BPP during 14,000 h in-situ test, the final ICR remained higher ($\sim 50 \text{ m}\Omega\cdot\text{cm}^2$ @1.4 MPa) than uncoated SS BPP ($\sim 25 \text{ m}\Omega\cdot\text{cm}^2$ @1.4 MPa). Moreover, since the PTL/MEA interface operates under stronger acidic conditions (pH = 0–3) than PTL/BPP interface (pH = 4–6), [18] the outermost layer of Ti, Ta and Nb on PTLs are expected to yield even greater ICR than on BPPs. These research evidence infer that because of their oxidation resistant behavior, PGMs [10,11] provide lower ICR than other transition metals (such as Ti, Nb, Ta)-based coatings on Ti PTL. The reason being the higher conductivity of PGMs (for e. g., Pt= 10^5 S/cm) [19] compared to TiO_2 (10^{-6} S/cm) [20], Nb_2O_5 (10^{-4} S/cm) [21] and $\text{TaO}_{x=2.21}$ ($1.9 \times 10^{-4} \text{ S/cm}$) [22] Hence the complete substitution of PGMs is not reasonable but their usage can be minimized by integrating them with less expensive transition metals.

Multi-layered coating with thin layer of one of the PGMs as a top layer and cost-effective transition metal as an interlayer offers a promising approach to control ICR without compromising PTL corrosion resistance. The reason for increased interest in multi-layered coatings stems from their ability to control properties of each individual layer by varying composition, thickness, number and order of deposition [23] Due to their densely compacted structure, the multi-layered coatings such as CrN/Ti, TiN/Ti etc. [24,25] exhibit lower density of pinholes and pores than single layered coatings, leading to higher corrosion resistance. In addition, multi-layered coatings with alternate hard/soft layers like TiN/Ti, brass/lead etc. show increased strength and hardness, better adhesion, and improved toughness than the single layered coatings [23,26] The higher hardness and toughness are attributed to dislocations pile up (known as Hall-Petch effect) [27] and the crack deflection [28] at the interface of hard/soft layers, respectively. The above findings establish the multiple advantages of multi-layered coatings over single layered coatings, leading to the next discussion of interlayer material used in the present study.

Compared to other transition metals (Mo, W) and alloys (SS, Inconel 625), Nb and Ta showed lowest current density and witnessed negligible weight loss before and after potentiostatic polarization test in the simulated PEMWE environment [29] Though Nb showed slightly higher current density (20 $\mu\text{A}/\text{cm}^2$ @2.0 V) than Ta (10 $\mu\text{A}/\text{cm}^2$ @2.0 V) at 70 °C, the lower cost of Nb (i.e. 1/4th of Ta) [30,31] makes it a promising candidate to be used as an interlayer between PGMs and PTL substrate. Moreover, Nb exhibits excellent corrosion resistance in H_2SO_4 solution due to the formation of stable Nb_2O_5 passive layer on its surface [32] Since fluoride ion (F^-) emission due to MEA degradation is a critical issue in PEMWE [33], the higher corrosion resistance of Nb compared to Ti [34] in the presence of F^- (0–0.24 M) provides an additional benefit. Next, various techniques such as magnetron sputtering [35], pulsed laser deposition [36], ion implantation [37] etc. have been used to deposit Nb-based coatings. Among these, DC magnetron sputtering is the simplest and most cost-effective method for deposition [38]

Our research group has previously worked on reducing Pt loading of commercial PTL by using transition metal as an interlayer between Pt and Ti PTL [36,39] Kalhori et al. [36] used pulsed laser deposition technique to deposit Nb (143 nm) and Pt (30 nm) on Ti PTL, achieving higher durability (5.5 h @2.0 A/ cm^2) than a single layered Pt (30 nm) on Ti PTL (4.5 h @2.0 A/ cm^2). The results showcased Nb's effectiveness as an interlayer, however the reported durability was significantly low, as shown above. Moradzadeh et al. [39] utilized sputter-coated NbTa-alloy (80 %Ta, 20 %Nb) as an interlayer (350 nm) between Pt (100 nm) and Ti PTL, achieving an exceptional durability of 117 h @2.0 A/ cm^2 . However, NbTa alloy interlayer used was 3.4 times more expensive than Nb [30,31] Moreover, the loading of Pt was twofold higher (100 nm) than that employed in the present study (50 nm). Lastly, Johar et al. [40] studied Nb/Ta multilayered coating (without Pt) on Ti BPP for PEM fuel cell application. The observed ICR was 7.2 $\text{m}\Omega\cdot\text{cm}^2$ @1.5 MPa after 6.0 h of CA test (@0.2 V, 80 °C), which was conducted in a relatively mild condition compared to standard CA test (@2.0 V, 80 °C) in PEMWE. Hence it can be stated that applying Nb/Ta multi-layered coating (without Pt) on Ti PTL would further elevate the ICR ($>10 \text{ m}\Omega\cdot\text{cm}^2$) due to the harsh PTL/MEA interface conditions, as discussed above. Considering the aforementioned results, this is the first time that sputtered Nb is being used as an interlayer between Pt and Ti PTL. Moreover, no other studies have previously investigated or compared the electrochemical behavior of co-deposited NbPt coatings with multi-layered counterpart.

Therefore, the objective of this work is to decrease the Pt loading of the PTL coating without sacrificing its durability and performance inside PEMWE. Hence to achieve this goal, the co-deposited and multi-layered NbPt coatings are sputtered on Ti PTL, with each having low Pt loading on their respective surface. NbPt coating combinations are initially evaluated against commercial PTL under ex-situ environment, followed by an in-situ comparison of best performing PTL sample with the commercial PTL in PEMWE cell.

2. Experimental

2.1. Coating materials

The coating configurations investigated in the present study are described below in Table 1 and Fig. 1.

Note that in A3-cd sample, the initial focus was to deposit single layer of NbPt co-deposition (without any Nb interlayer) with similar thickness (400 nm) and Pt loading as A4-ml sample. However, due to its softer nature, Pt deposition rate was higher than Nb at constant power, leading to greater Pt loading in A3-cd than A4-ml. Despite the multiple efforts to reduce Pt to Nb deposition ratio by maximizing Nb sputtering power (250 W) and lowering Pt power, Pt loading remained higher for A3-cd. Therefore, Nb interlayer of 250 nm was selected, and the top layer was deposited using NbPt co-deposition, maintaining a Nb to Pt deposition rate ratio of 2:1 by setting the powers to 250 W and 60 W, respectively. This led to similar Pt loading and total thickness in both A3-cd and A4-

Table 1
Description of the samples' coatings corresponding to their sample ids.

Sample id	Sample details
A1-un	Uncoated Ti PTL (2GDL06N-015 BQ), purchased from Bekaert
A2-nb	Single layered coating of Nb (400 nm) on Ti PTL
A3-cd	Multi-layered coating, with Nb as an interlayer (250 nm) and co-deposition of Nb and Pt as a top layer (150 nm) on Ti PTL. The total coating thickness is 400 nm
A4-ml	Multi-layered coating, with Nb as an interlayer (350 nm) and Pt as a top layer (50 nm) on Ti PTL. The total coating thickness is 400 nm. Note that the Pt loading is same in both A3-cd and A4-ml
A5-cmc	Commercially coated PTL (Bekaert 2GDL06N-0250-PT200), with single layer of Pt (200 nm)

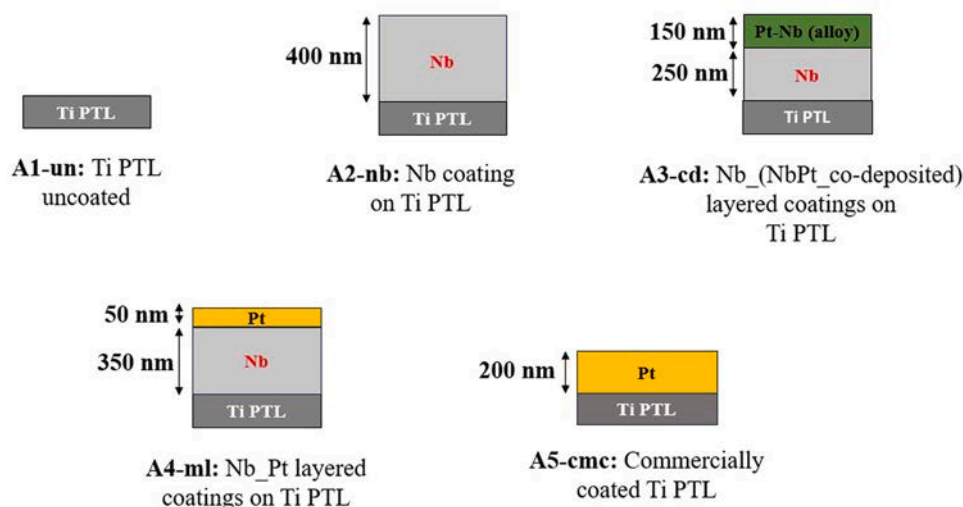


Fig. 1. Schematic of different types of coatings along with their thicknesses, as coated on Ti PTL.

ml. Nevertheless, as will be discussed later in Section 3.2.2, increasing the thickness of NbPt co-deposited top layer does not improve the corrosion resistance of A3-cd.

2.2. Pre-treatment

Before coating each sample, a three-steps cleaning procedure was adopted for the uncoated Ti PTLs. First, the PTLs were heated in deionized water (DI) water (18.2 MΩ.cm) at 80 °C for 15 min to dissolve the water-soluble impurities. Then, they were ultrasonically cleaned in an acetone and ethanol solution for 15 mins to detach greasy substance, if any, from the surface and pores of the PTLs. Again, they were heated in the DI water at 80 °C to evaporate ethanol (boiling point = 78 °C) from the surface of the PTLs. Finally, PTLs were left in the room temperature to dry.

2.3. Coating technique and thickness measurement

These Ti PTLs were then coated on both sides using magnetron sputtering. Once both Pt and Nb targets were installed, Ar gas was passed through chamber under external power supply. The base pressure and working pressure were maintained at 1.33×10^{-4} Pa and 6.66×10^{-1} Pa, respectively. The deposition power was kept constant at 150 W for both Pt and Nb targets. However, in the case of NbPt co-deposition, Nb was deposited at higher power (250 W) than that of Pt (60 W). This was done to achieve a Nb:Pt deposition ratio of 2:1, ensuring similar Pt loading in both A3-cd and A4-ml sample. The sputtering procedure used here was thickness-controlled rather than time-controlled. It means that coating thickness was monitored using built-in 14 mm Au crystal. In addition, thickness was measured through cross-sectional imaging in focused ion beam (FIB) technique. Thermo Scientific Helios 5 (FIB) was used to generate high Ga ions currents to micro-machine (milling) PTL's cross section. Note that, before machining, the local area of interest was deposited with carbon, to protect coating's top layer from destructive nature of Ga ion beam. Figure S1a, b in Supplementary Information shows FIB images of surface milling and thickness measurement, respectively.

2.4. Electrochemical tests

Three-electrode setup was used to study and compare the electrochemical behavior of the coatings. This setup was connected to SP 300 Biologic Potentiostat to record performance of the coating in a simulated PEMWE environment. A 0.5 M H₂SO₄ solution was used as an electrolyte

for the test. Sample to be studied (1.0 cm × 1.0 cm exposed area) was used as a working electrode, along with graphite rod and Hg/Hg₂SO₄ (615 mV vs NHE) electrode, which were used as a counter and reference electrode, respectively. The hot water (80 °C) was circulated around the water jacketed beaker (Pine Instruments Inc.) to maintain a constant setup temperature of 80 °C. Initially, before measurement, the samples were kept at open circuit potential (OCP) for 4.0 h, to reach dynamic equilibrium with the surrounding. Then, samples were subjected to Potentiodynamic polarization technique (potential sweep of −0.8 V to 0.8 V w.r.t OCP at 1.0 mV/s scan rate) to study coatings anti-corrosion capability. Finally, Potentiostatic polarization i.e. Chronoamperometry (CA) test was performed at 2.0 V_{RHE} for 6.0 h to compare coating stability under corrosive environment. Note that each electrochemical test was repeated at least three times on each type of the PTL samples.

2.5. Durability test

To monitor long-term durability of each sample, End of life (EOL) test was performed at 80 °C. An in-house two electrode setup (graphite rod as counter electrode) was used in connection with DC source, which supplied current density of 2.0 A/cm². At the end of the test, Voltage values were plotted with time. Sudden change in slope of an output voltage was taken as the end of life of the PTLs. Note that care has been taken to make sure that the volume of H₂SO₄ solution remained same throughout the test. This was to keep the exposed area constant at 1.0 cm².

2.6. Physical characterization techniques

The change in surface morphology of PTLs (after electrochemical tests) were investigated through Hitachi VP-SEM SU1510, enabled with scanning electron microscopy (SEM) and energy dispersive x-ray spectroscopy (EDS) capabilities. EDS measurement was done to monitor change in elemental composition and degradation level in the coatings. Furthermore, the quantitative analysis of surface oxides was performed using X-Ray Photoelectron Spectroscopy (XPS) spectra. PHI Quantes instrument was used to bombard electrons on Al anode, producing k-alpha radiations of 1486.6 eV. These radiations were then used to identify oxidation states of the surface element. The XPS data obtained was then processed using CasaXPS software and the binding energy was calibrated using C 1 s peak (284.8 eV) to make sure all energies values are shifted to a correct position. Surface contact angle of multi-layered (A4-ml) and commercially coated (A5-cmc) samples was measured using Kruss Mobile Surface Analyzer. Its inbuilt software was then used

to calculate contact angle (θ) of water droplet using circle method [43] The surface roughness of A4-ml and A5-cmc samples were investigated through VK-X3000, Keyence laser microscope. For each sample, three areas were scanned to calculate mean roughness.

The ICR of the PTLs were measured as a function of the compaction pressure (0.5 to 4.0 MPa), generated by the ZwickRoell tester. Before measurement, sample was kept between two carbon Gas diffusion layers (GDLs) and was then compressed between the gold coated Cu plates. A constant current of 2.0 A was passed and a corresponding drop in voltage was recorded at each of the set pressure values. Finally, ICR was calculated using equation,

$$\text{Resistance (ICR)} = (\text{Voltage} \times \text{Area}) / \text{Current} \quad (1)$$

Here, Area denotes the contact area of the sample (taken as 1.0 cm^2). It should be specified that the care has been taken to accurately measure the ICR of the coatings by adopting the method followed by Wang H [41] According to which, another ICR measurement was performed, in which only one carbon GDL was kept between two gold coated Cu plates. The value of ICR obtained in the latter case was deducted from the total ICR measured in the case of PTLs. Subsequently, this ICR value was further halved to get the correct value of the ICR between carbon GDL and PTL.

2.7. In-situ test

In situ testing of commercially coated (A5-cmc) and multi-layered (A4-ml) samples were performed in Scribner's PEMWE cell. The test employed a Nafion 115 membrane, in-house coated with Ir catalyst (loading = 1.0 mg/cm^2) on anode and Pt/C catalyst (loading = 0.5 mg/cm^2) on cathode. The PTL (5.0 cm^2) and commercial carbon GDL were kept on anode and cathode side, respectively. The cell temperature was set at 80°C . The polarization curve was recorded by ramping up the current density from 0.01 A/cm^2 to 2.0 A/cm^2 at every 5.0 mins interval. That is, from 0.01 A/cm^2 to 0.02 A/cm^2 in the steps of 0.002 A/cm^2 , then 0.02 A/cm^2 to 0.1 A/cm^2 in the steps of 0.02 A/cm^2 , from 0.2 A/cm^2 to 1.2 A/cm^2 in the steps of 0.1 A/cm^2 and at last from 1.2 A/cm^2 to 2.0 A/cm^2 in the steps of 0.2 A/cm^2 . In addition, electrochemical impedance spectroscopy (EIS) was captured at each of these current densities between 0.01 Hz and 100 kHz.

3. Results and discussion

3.1. SEM surface morphology

The surface (Fig. 2) and cross-sectional (Figure S1b in Supplementary Information) characteristics of all pristine samples are discussed hereafter. Fig. 2a shows SEM morphological micrograph of uncoated Ti PTL (Ti-un) whereas Fig. 2b-d represent micrographs for in-house coated samples before corrosion tests. Fig. 2b-d shows that coatings are homogeneous, dense, and are free from any kind of visible defects such as pinholes and cracks. Note that bumpy features on each fiber is due to the inherent design of Ti felt substrate and must not be attributed to coating morphology. Next, Figure S1b shows cross-sectional view of coated samples. Notably, layers (with different density contrasts) of Nb and co-deposited NbPt in A3-cd and that of Nb and Pt in A4-ml are compact and have well-defined interfaces between them. The transition between the layers is continuous and coatings seem to be well-adhered to the substrate. Above observations infer that these coatings will act as a compact solid interface between corrosive medium and Ti substrate, preventing the direct flow of acid electrolyte (present inside the PEMWE) to the Ti surface. Next, in A5-cmc (Fig. 2e), the coating appears to exhibit globular structure that differs from the coating morphology observed in the other samples. Since no information is available about the commercial coating procedure used, no further remarks are made on coating characteristics. The SEM micrographs at low magnifications of each sample are shown in Supplementary Information (Figure S2).

3.2. Electrochemical measurement analyses

3.2.1. Open circuit potential (OCP)

OCP, known as zero-current potential (ZCP) is a method for obtaining corrosion potential when sample reaches dynamic equilibrium with the surroundings [42] Fig. 3 shows OCP curves of the samples. A1-un (-1.15 V) exhibits lowest OCP followed by A2-nb (-0.24 V), A3-cd (0.151 V), A4-ml (0.157 V) and A5-cmc (0.199 V). This suggests that the uncoated Ti PTL (A1-un) is most susceptible to corrosion in $0.5 \text{ M H}_2\text{SO}_4$ solution due to the dissolution of Ti oxide (TiO_{2-x}) passive layer [15] However, for A2-nb, Nb_2O_5 passive layer formation suppresses an OCP drop to -0.62 V before achieving dynamic equilibrium at -0.24 V . Next, for A3-cd, the co-existence of both Nb and Pt in top layer (Figure S3, S4 in Supplementary Information) leads to continuous formation of Nb oxide passive films, delaying the voltage stabilization in

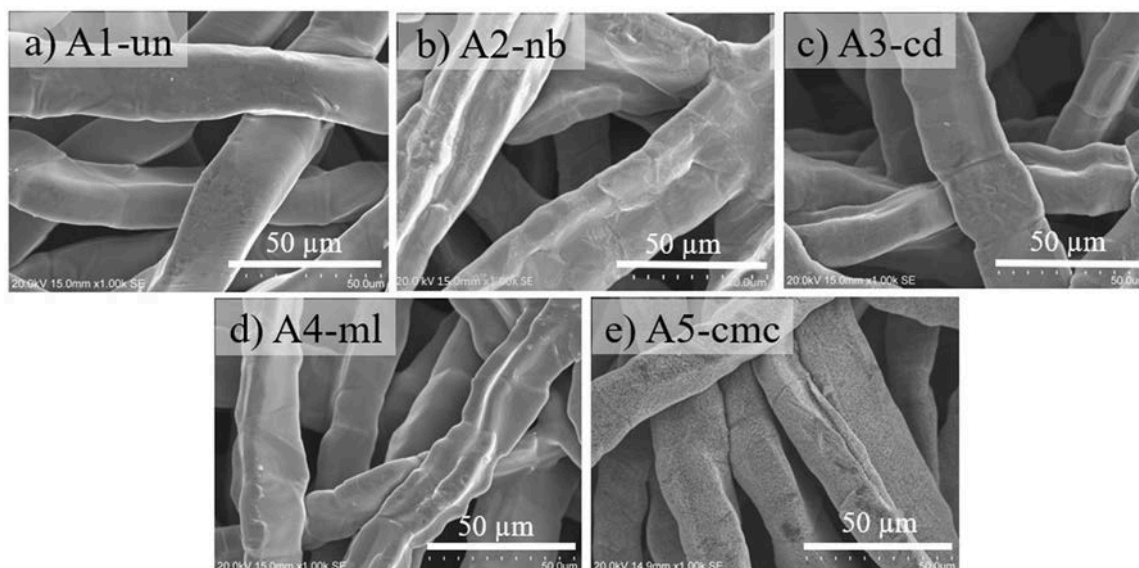


Fig. 2. SEM micrographs depicting the surface morphology of each pristine sample at 1000X.

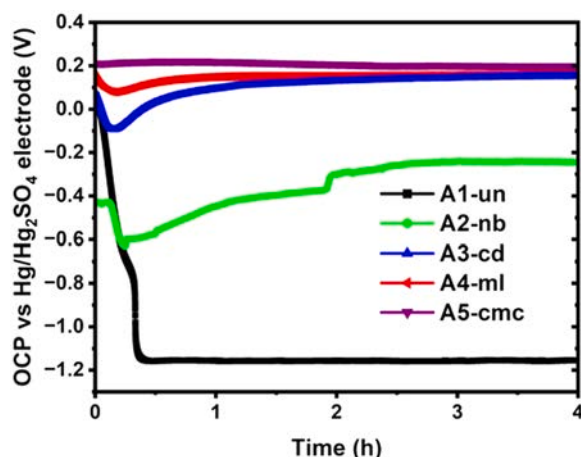


Fig. 3. OCP curves of the samples A1-un, A2-nb, A3-cd, A4-ml and A5-cmc in 0.5 M H_2SO_4 solution at 80 °C.

A3-cd (3.0 h) compared to A4-ml (1.0 h). Note that given their noble characteristics, coatings with Pt top layer i.e. A4-ml and A5-cmc shows the highest OCP after 4 h of exposure.

3.2.2. Potentiodynamic polarization

Fig. 4 shows the Potentiodynamic polarization curve for all the samples. The potentiodynamic technique is used to study kinetics of the corrosion process. The computed values of corrosion potential (E_{corr}), corrosion current density (I_{corr}), tafel slopes (β_a and β_c) and polarization resistance (R_p) are shown in Table 2. Tafel slopes are determined using ‘Tafel fit’ tool from EC-lab software, within 60 mV potential range on either side of the E_{corr} [15]. The I_{corr} and R_p are calculated using Tafel extrapolation method and Stern-Geary equation respectively. Table 2 indicates that A2-nb exhibits a substantially reduced corrosion rate ($R_p = 1792.5 \pm 94.6 \Omega \cdot \text{cm}^2$) than A1-un ($R_p = 10.3 \pm 0.7 \Omega \cdot \text{cm}^2$). The observation aligns with the study done by Carmo et al. [43], which demonstrated that Nb has greater corrosion resistance than Ti in H_2SO_4 due to the stable Nb_2O_5 passive film on the Nb surface. The high value of R_p in the case of A2-nb is consistent with SEM micrograph (Fig. 5b) and EDS elemental analysis (Fig. 5f-i) after CA test. Fig. 5b indicates negligible amount of chipping or peeling of the Nb coating off the Ti substrate, which is in line with the low contrast Backscattered electron (BSE) image of A2-nb (Fig. 5f). The absence of Z contrast denotes the presence of only one element or compound on top surface namely, Nb

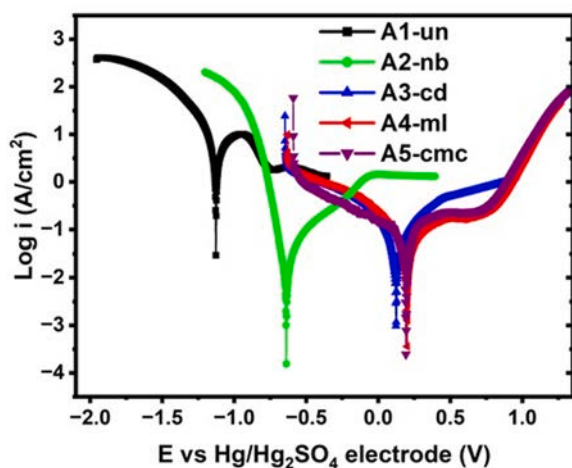


Fig. 4. Potentiodynamic polarization curves of the samples A1-un, A2-nb, A3-cd, A4-ml and A5-cmc in 0.5 M H_2SO_4 solution at 80 °C.

Table 2

Corrosion parameters (mean \pm standard deviation) of the samples calculated from potentiodynamic polarization curve.

Samples	E_{corr} (V)	I_{corr} ($\mu\text{A}/\text{cm}^2$)	β_a (mV/decade)	β_c (mV/decade)	R_p ($\Omega \cdot \text{cm}^2$)
A1-un	-1.125 ± 0.077	2404.08 ± 138.35	157 ± 5	89 ± 2	10.3 ± 0.7
A2-nb	-0.637 ± 0.023	7.86 ± 0.42	74 ± 3	58 ± 1	1792.5 ± 94.6
A3-cd	0.122 ± 0.008	19.40 ± 1.14	94 ± 1	95 ± 3	1058.7 ± 67.9
A4-ml	0.204 ± 0.018	13.12 ± 0.39	92 ± 2	91 ± 1	1518.2 ± 44.3
A5-cmc	0.192 ± 0.031	17.19 ± 0.52	110 ± 4	92 ± 3	1257.1 ± 38.8

oxides in the present case (see Fig. 5g-i). Therefore, the SEM and EDS analyses of A2-nb indicate that the Nb oxide formed is stable under acidic media and Nb has good adhesion on Ti surface.

For A4-ml, since Pt has a lower affinity for O_2 compared to that of Ti, its R_p value ($1518.2 \pm 44.3 \Omega \cdot \text{cm}^2$) is greater than A1-un. Moreover, due to its lowest ($0.179 \text{ mA}/\text{cm}^2$) passivation current density (I_{pass}) (Fig. 4), A4-ml has the highest chemical stability than other samples. This statement is consistent with the SEM image of A4-ml (Fig. 5d), which shows negligible peeling of Pt coating, indicating good adhesion of Pt with Nb. However, in the case of A3-cd (Fig. 5c), substantial coating delamination was observed after the CA, explaining the instability of I_{pass} . This behavior could be attributed to poor adhesion of Pt with Nb oxides. It has been reported that due to Pt's inability to form oxide bonds, it tends to adhere poorly with metal oxides like TiO_2 [44], Al_2O_3 [45]. In view of this, Pt is likely to exhibit suboptimal adhesion with Nb_2O_5 passive layer, co-existing in the top layer. Another contributing factor could be residual stress or strain, owing to non-uniform Pt and Nb deposition rate in A3-cd. Moreover, since the atomic size of both Nb and Nb_2O_5 ($2.69 \times \text{Volume}_{\text{Nb}}$) [46] is greater than Pt, it further enhances the lattice strain in A3-cd sample. Nevertheless, it must be emphasized here that even if we had increased the thickness of the co-deposited top layer in the A3-cd sample, it would likely have had little to no positive impact on the adhesion or strain of the coatings. Lastly, A5-cmc shows higher amount of peeling (Fig. 5e) compared to A4-ml (Fig. 5d), which is in accordance with their corresponding R_p values. This could be attributed to poor adhesion of Pt with Ti, which is much more apparent in the SEM images after EOL test (Fig. 9b). Hence, it will be discussed in detail in Section 3.4. The SEM micrographs at low magnifications for all the samples (Figure S5) after the CA test are shown in Supplementary Information.

3.2.3. Potentiostatic polarization (CA)

CA is used to investigate the electrochemical stability of protective coatings by measuring the variation of current response with time under the application of continuous constant voltage to the working electrode. Therefore, CA test (Fig. 6) was conducted in 0.5 M H_2SO_4 solutions for 6.0 h at 2.0 V to simulate the PEMWE anodic conditions. The order of current densities after 6.0 h of CA is A5-cmc ($110 \text{ mA}/\text{cm}^2$) > A4-ml ($90 \text{ mA}/\text{cm}^2$) > A3-cd ($86 \text{ mA}/\text{cm}^2$) > UN-Ti ($0.68 \text{ mA}/\text{cm}^2$) > A2-nb ($0.18 \text{ mA}/\text{cm}^2$). The initial decrease in the current density could be attributed to formation of passive oxide film on the surface of each sample [15]. The immediate stabilization of current density in the case of A1-un (250 s) and A2-nb (150 s) indicates faster kinetics for the formation of passive oxide film in both the cases. Interestingly, the higher current density (after 6.0 h) observed in the case of A4-ml ($90 \text{ mA}/\text{cm}^2$) compared to A3-cd ($86 \text{ mA}/\text{cm}^2$), doesn't indicate its lower corrosion resistance, but represents higher OER activity on Pt surface. In fact, the current densities of any two samples, with different surface composition and roughness should not be correlated directly with their corrosion resistance, as the contribution from OER activity will be different in both the

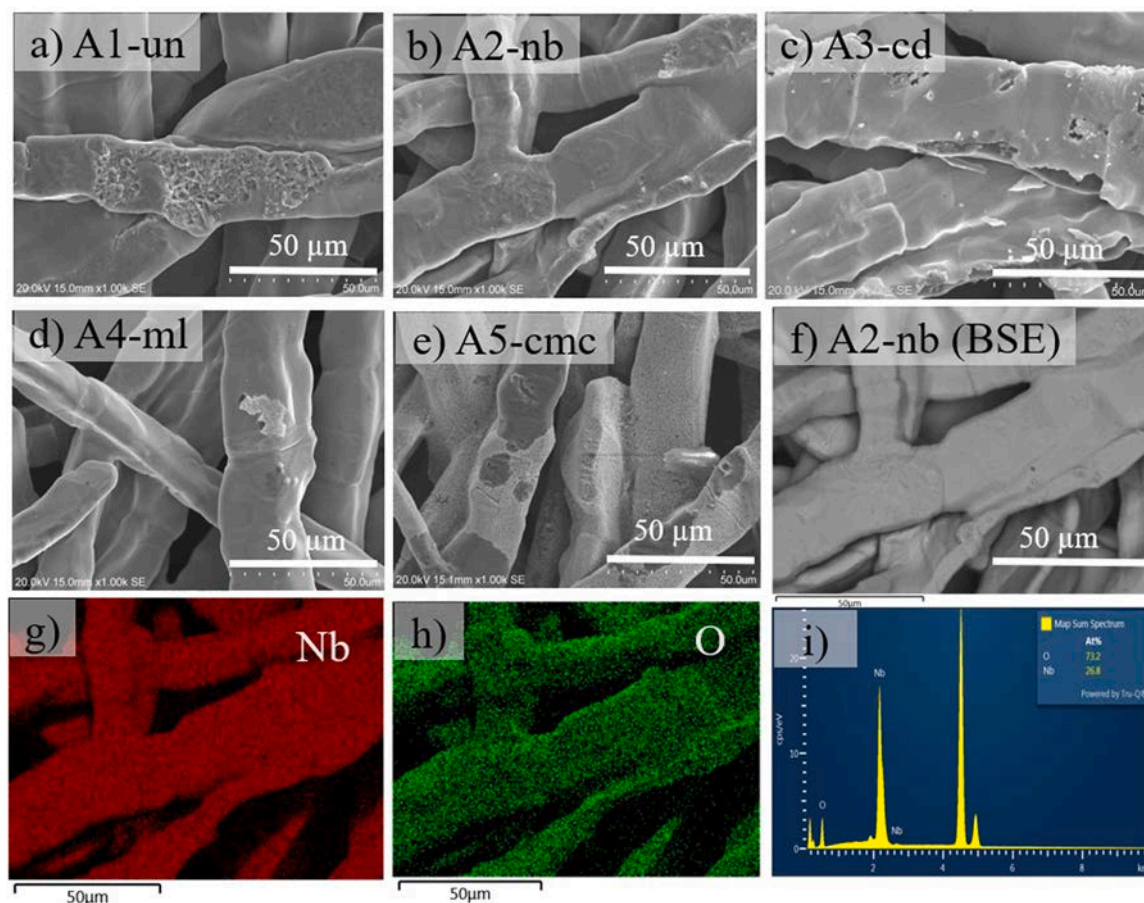


Fig. 5. (a-e) SEM micrographs of the samples A1-un, A2-nb, A3-cd, A4-ml and A5-cmc respectively after the chronoamperometry (CA) test (f) Backscattered electron (BSE) image of the sample A2-nb (g-i) SEM/EDS analysis of A2-nb after CA test.

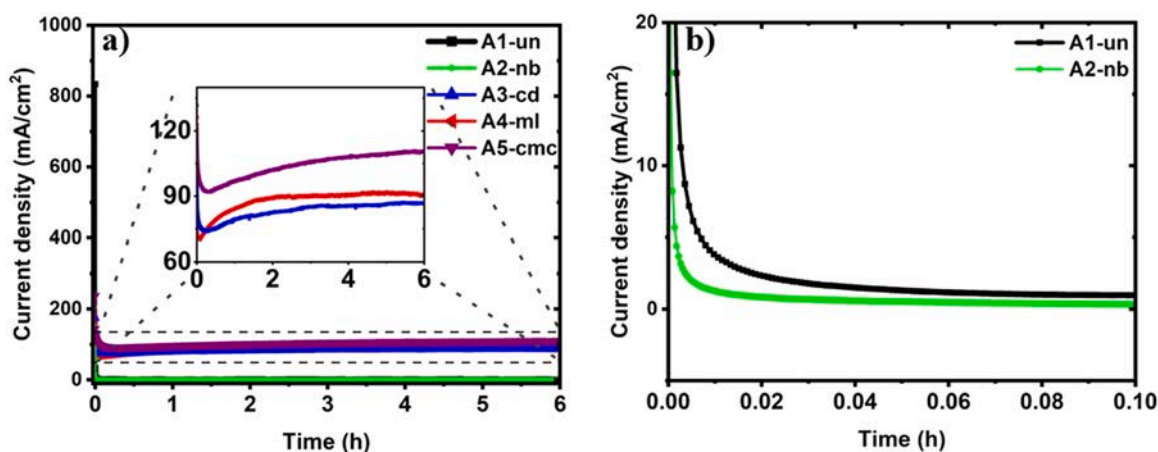


Fig. 6. (a) Potentiostatic polarization curves (under 2.0 V_{RHE}) of all the samples (A1-un, A2-nb, A3-cd, A4-ml and A5-cmc) in 0.5 M H₂SO₄ solution at 80 °C (b) Magnified view for A1-un and A2-nb portraying the stability time for each sample.

cases. In view of this, in the case of A5-cmc sample, since no information is given on the company's website about the deposition technique used, no comments can be made about the OER activity. But, as seen from Fig. 2e, since the surface characteristics in the case of A5-cmc is different than A4-ml (Fig. 2d), the OER activity is assumed to be different in both the cases. Therefore, for the comparison purposes, observation from SEM (Fig. 5), R_p values (Table 2) and durability test (discussed later) will be more conclusive than the CA data in the specific case of different top surfaces exposed to corrosive environment.

3.3. Interfacial contact resistance (ICR) measurement analyses

In addition to high corrosion resistance, PTL is required to have good surface conductivity with BPP and MEA inside the PEMWE stack. Hence, ICR measurement is done to compare PTLs surface conductivities in the compression range of 1.2 to 2.0 MPa, which is a typical pressure range used for assembling commercial stacks [35]. Fig. 7 shows the ICR of each sample before and after 6.0 h of CA test. In Fig. 7a, the ICR order for the entire pressure range is A1-un > A2-nb > A3-cd > A4-ml > A5-cmc. The

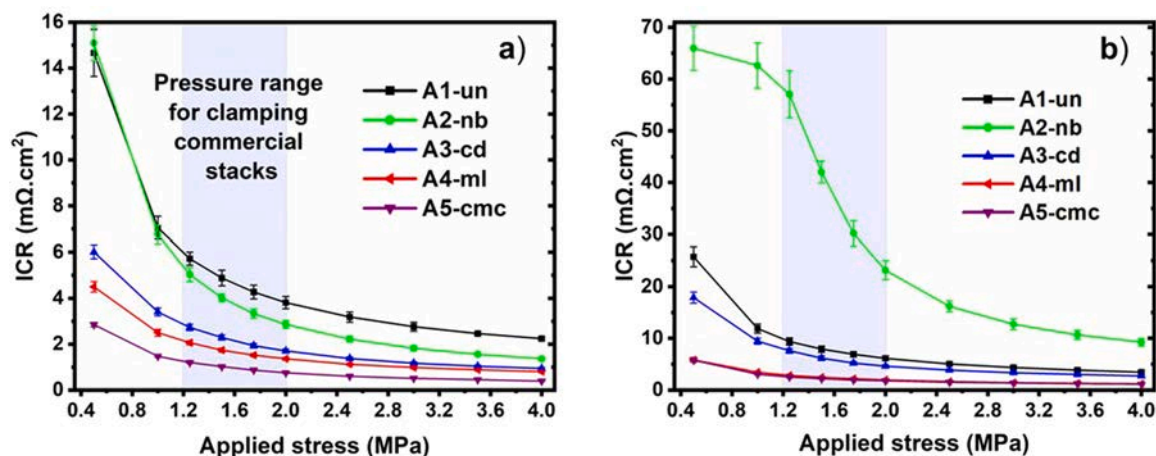


Fig. 7. ICR measurements of the samples (A1-un, A2-nb, A3-cd, A4-ml and A5-cmc) (a) before and (b) after 6.0 h of CA test at 2.0 V. The error bars depict the individual standard deviation corresponding to each value.

underlying cause of this trend is addressed hereafter. The lower conductivity of TiO_2 (10^{-6} S/cm) [20] compared to Nb_2O_5 (10^{-4} S/cm), [21] explains the ICR order of first two cases. Next, due to Pt's noble nature, [47] both A4-ml and A5-cmc exhibit low ICR i.e. $1.88 \text{ m}\Omega\cdot\text{cm}^2$ @1.4 MPa and $1.12 \text{ m}\Omega\cdot\text{cm}^2$ @1.4 MPa, respectively. However, the higher surface roughness of A4-ml (Average roughness (S_a) = $5.76 \mu\text{m}$) compared to A5-cmc (S_a = $5.29 \mu\text{m}$) (Figure S6 in Supplementary Information) leads to increased ICR in the former. Note that due to the limited information on the commercial coating methodology, the other possible factors contributing to low ICR in A5-cmc remain unknown to authors. Lastly, due to the co-existence of Pt and Nb in A3-cd top surface (Figure S3, S4 in Supplementary Information), ICR curve lies between A2-nb and A4-ml.

Fig. 7b shows the ICR after 6.0 h of CA test at 2.0 V. The order of ICR remains same for all the samples except A2-nb, which shows considerably higher ICR ($50.41 \text{ m}\Omega\cdot\text{cm}^2$ @1.4 MPa) than the uncoated Ti substrate (A1-un) ($8.12 \text{ m}\Omega\cdot\text{cm}^2$ @1.4 MPa). This observation is in line with the study done by Huatao et al., [15] who demonstrated that Nb/NbN multi-layered sample (thickness = 600 nm), with NbN as a top layer exhibited higher ICR than the uncoated Ti BPP substrate. But due to higher conductivity of NbN (10^4 S/cm) [48] than Nb_2O_5 (10^{-4} S/cm), the ICR values obtained by the author ($31.45 \text{ m}\Omega\cdot\text{cm}^2$ @1.4 MPa) was slightly lower than the present case of A2-nb ($50.41 \text{ m}\Omega\cdot\text{cm}^2$ @1.4 MPa). However, note that based on the conductivities of Nb_2O_5 and TiO_2 (mentioned above), ICR of A2-nb should be lower than A1-un. The contradictory observation indicates thick passive layer formation in the case of A2-nb, resulting in an increase in ICR. Kellenberger et al. [49] showed that the Nb_2O_5 passive layer thickness increased from 1.7 nm to 8.1 nm after 6.0 h of CA test at 90°C , resulting in high value of ICR after corrosion test. The ICR difference between the current ($50.41 \text{ m}\Omega\cdot\text{cm}^2$ @1.4 MPa) and previous ($345 \text{ m}\Omega\cdot\text{cm}^2$ @1.4 MPa) [49] work is attributed to distinct experimental parameters like temperature, O_2 saturation level, substrate type (metallic Nb), and the surface morphology of substrate used in the latter.

Note that despite exhibiting higher ICR, the percentage increase in ICR from before to after CA test is lower in A4-ml (42 % @1.4 MPa) than A5-cmc (110 % @1.4 MPa). This statement is consistent with greater peeling in A5-cmc than A4-ml, as discussed above (Fig. 5d,e). Nevertheless, it must be emphasized that within the pressure range of 1.2 to 2.0 MPa, all the samples except A2-nb satisfy the DOE target ($<10 \text{ m}\Omega\cdot\text{cm}^2$) set for PEM fuel cell (the target value on a similar line can be expected for PEMWE stack as well). As shown in the Fig. 7, the ICR at 1.4 MPa for A1-un, A2-nb, A3-cd, A4-ml and A5-cmc before CA is $5.34 \text{ m}\Omega\cdot\text{cm}^2$, $4.57 \text{ m}\Omega\cdot\text{cm}^2$, $2.51 \text{ m}\Omega\cdot\text{cm}^2$, $1.88 \text{ m}\Omega\cdot\text{cm}^2$ and $1.12 \text{ m}\Omega\cdot\text{cm}^2$, respectively, which after CA has increased to $8.12 \text{ m}\Omega\cdot\text{cm}^2$, $50.41 \text{ m}\Omega\cdot\text{cm}^2$, $6.85 \text{ m}\Omega\cdot\text{cm}^2$, $2.67 \text{ m}\Omega\cdot\text{cm}^2$ and $2.35 \text{ m}\Omega\cdot\text{cm}^2$, respectively.

cm^2 , $6.85 \text{ m}\Omega\cdot\text{cm}^2$, $2.67 \text{ m}\Omega\cdot\text{cm}^2$ and $2.35 \text{ m}\Omega\cdot\text{cm}^2$, respectively.

3.4. End of life analyses

End of life is an important test from the perspective of reviewing both corrosion resistance and electrical conductivity of the PTLs at the same time. During the test, constant current density of $2.0 \text{ A}/\text{cm}^2$ is applied and corresponding output voltage is recorded (Fig. 8). It is observed that as electrical conductivity decreases (either due to passivation or deterioration), a higher output voltage is needed to sustain $2.0 \text{ A}/\text{cm}^2$. Hence, the time at which the voltage begins to increase exponentially is defined as the end of life of sample. A1-un and A2-nb show shorter life span of 2.0 and 2.5 mins (Fig. 8 Inset), indicating rapid passive oxide layer formation on Ti and Nb surface, respectively. While in the case of A3-cd, the coexistence of Nb and Pt suppresses the amount of Nb oxide on the surface, resulting in a higher conductivity (17 h) than A2-nb.

Next, A4-ml shows exceptionally high life span value of 102 h compared to 15 h in the case of A5-cmc sample. This could be interpreted in three different ways. Firstly, it could be attributed to the poor adhesion of Ti with Pt (Fig. 5e) compared to the adhesion of Nb with both Pt (Fig. 5d) and Ti (Fig. 5f), as discussed above in Section 3.2.2. These findings are further reinforced by SEM (BSE image) for both samples after 15 h of exposure time (Fig. 9a,b). A5-cmc is peeled off to a greater extent compared to A4-ml, where negligible peeling is observed on the surface. Secondly, this may be a consequence of higher contact

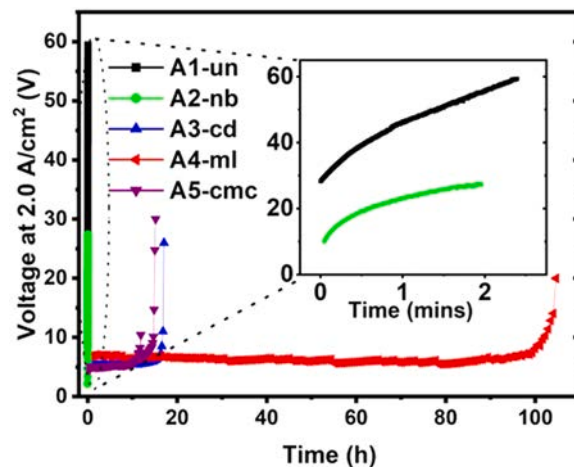


Fig. 8. End of Life analysis of the samples (A1-un, A2-nb, A3-cd, A4-ml and A5-cmc) conducted at $2.0 \text{ A}/\text{cm}^2$ in $0.5 \text{ M H}_2\text{SO}_4$ solution at 80°C .

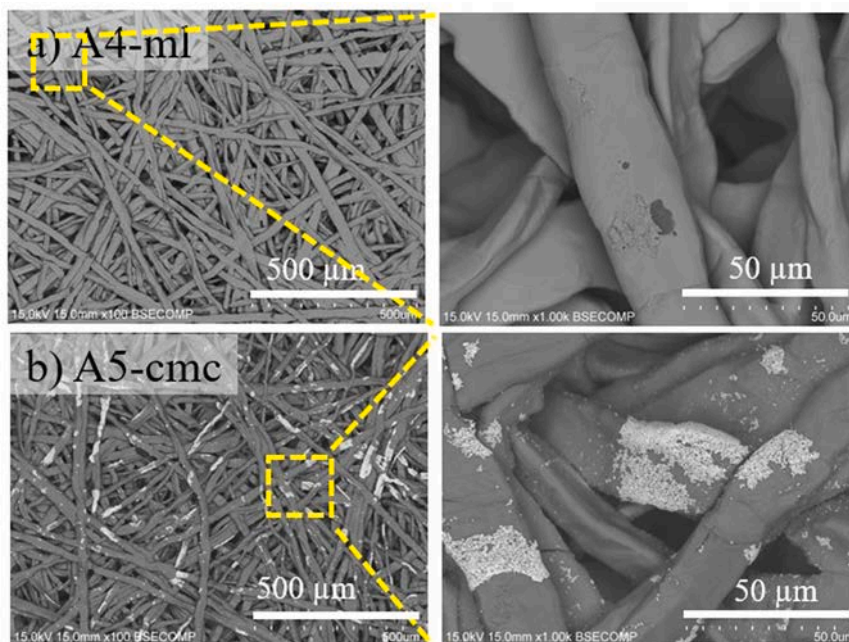


Fig. 9. SEM (BSE) micrographs of the samples (a) A4-ml and (b) A5-cmc after 15 h of End of Life test at 2.0 A/cm².

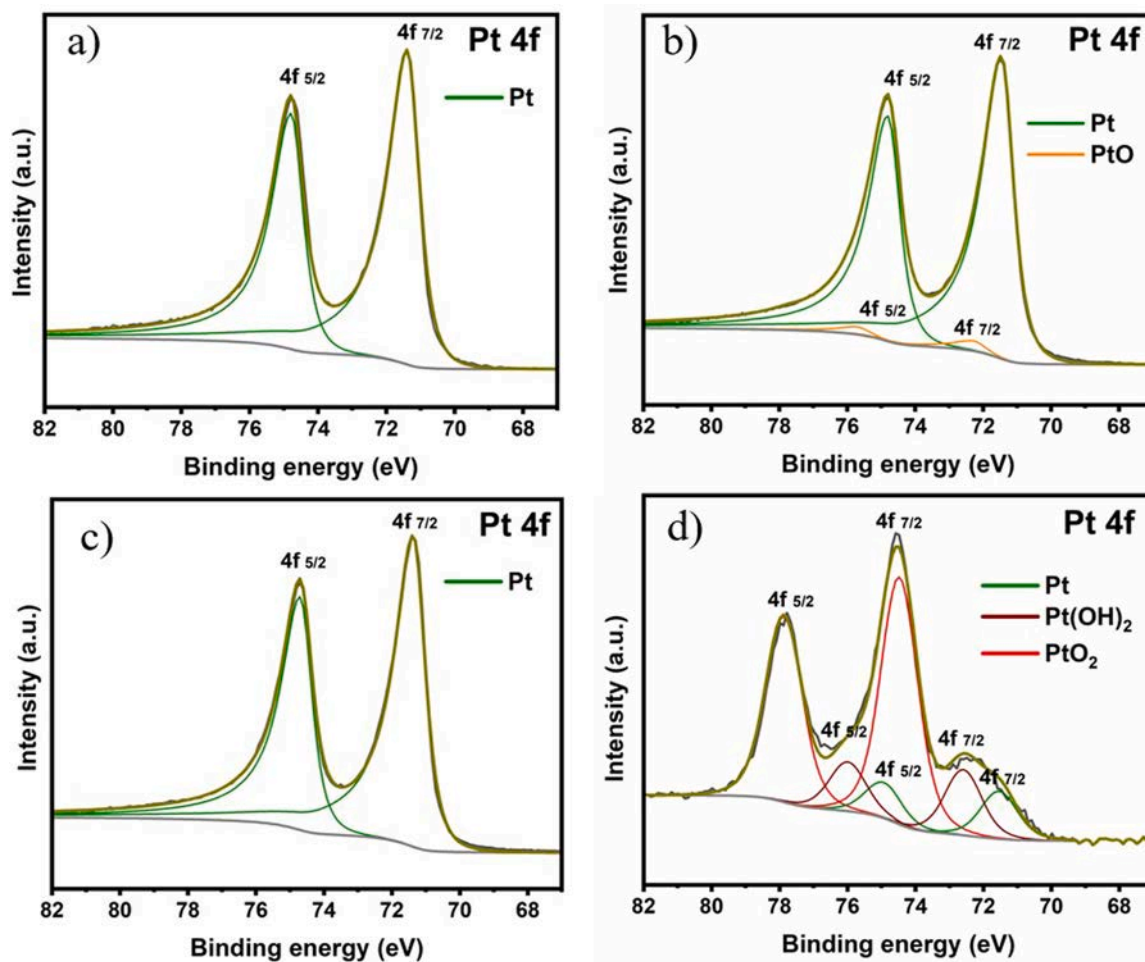


Fig. 10. X-Ray Photoelectron Spectroscopy (XPS) analyses for A4-ml (a) before and (b) after 15 h of End of Life (EOL) test and for A5-cmc (c) before and (d) after 15 h of EOL test.

angle of A4-ml ($\theta=132^\circ$) compared to A5-cmc ($\theta=120.5^\circ$) (Figure S7a,b in Supplementary Information), indicating greater hydrophobicity. Owing to its lower interaction with corrosive medium, A4-ml exhibits higher corrosion resistance than A5-cmc. Lastly, because of their densely compacted structure, multi-layered coatings have lower density of pinholes and pores than single layered coatings [24,25,50]. The higher number of pinholes in single layered coatings allows the electrolyte to reach the substrate with ease [50], causing the formation of galvanic couple between the coating and substrate material. This essentially means that the less noble material out of the two corrodes faster in comparison to the decoupled state. Considering all the above-mentioned scenario, similar phenomenon is likely to hold in commercial sample (A5-cmc). Since Pt is more noble than Ti, the local anodic oxidation of Ti would get enhanced because of the large cathodic area provided by the Pt top surface. Hence it can be stated that the introduction of Nb as an interlayer in the case of A4-ml, essentially decreases galvanic coupling effect between the Pt and Ti, by reducing the direct flow of electrolyte to the substrate. Note that the only way the electrolyte solution could directly reach the substrate is when the pinholes present in the top layer of Pt aligns perfectly with the pinholes present in the Nb [51]. Hence, the effective number of diffusive paths to the substrate decreases in case of A4-ml confirming its higher EOL compared to A5-cmc.

Next, XPS is done to study Pt's oxidation state on their respective surfaces. Fig. 10 shows the XPS spectra of Pt 4f for A4-ml and A5-cmc samples, both before and after 15 h of exposure time. Depending on Pt's oxidation state, the XPS spectrum is split into four different Pt components i.e., Pt (0), PtO/Pt(OH)₂ (+2) and PtO₂ (+4). The binding energy (B.E.) corresponding to the Pt 4f 7/2 peaks of Pt (0), PtO, Pt(OH)₂ and PtO₂ are 71.4 eV, [52] 72.3 eV [53], 72.6 eV [54], and 74.6 eV [55], respectively with $\Delta = 3.3$. Table 3 shows the relative composition of Pt and its oxides, acquired from curve fitting software. It is evident that both A4-ml and A5-cmc samples are initially coated with metallic Pt, which partially converts to Pt oxide phases after 15 h of EOL test. For instance, in A4-ml, most of the Pt is in metallic state (95.89 %) and the rest is in PtO (4.11 %), whereas in A5-cmc, most of the Pt is in PtO₂ (68.58 %) and the rest is in Pt(OH)₂ (18.22 %) and metallic Pt (13.20 %) state. Since the conductivities of Pt(+2) (10³ S/cm) and Pt(+4) (1.0 S/cm) are lower compared to Pt(0) (10⁵ S/cm), [19] the large percentage of Pt oxides explains the premature voltage shoot up in A5-cmc compared to A4-ml. Moreover, besides Pt oxidation, exposed area of Ti (as seen in Fig. 9b) also gets oxidized, cascading down the coating conductivity, leading to shorter EOL in A5-cmc. Note that an intermediate XPS analysis was also conducted for A5-cmc at the midpoint of its EOL (i.e. after 7.5 h) to investigate its behavior under stable voltage condition. However, its oxide content remained higher (Pt=76.06 %, PtO=23.94 %) compared to A4-ml (after 15 h of EOL) as shown in Figure S7c in Supplementary Information.

Based on ex-situ testing, it can be concluded that the NbPt co-deposited coatings have lower corrosion resistance, shorter durability and higher ICR compared to multi-layered NbPt coatings, which is compared next with commercial sample in the in-situ conditions of PEMWE.

Table 3

Quantitative analysis (atomic percentage) of Pt and its oxides for A4-ml and A5-cmc both before and after 15 h of End of Life test.

Samples	FWHM (eV)	Pt (%)	PtO (%)	Pt(OH) ₂ (%)	PtO ₂ (%)
A4-ml (before)	0.81	100	–	–	–
A4-ml (after 15 h)	0.83	95.89	4.11	–	–
A5-cmc (before)	0.82	100	–	–	–
A5-cmc (after 15 h)	1.21	13.20	–	18.22	68.58

3.5. In-situ analyses

The commercial PTL (A5-cmc) consists of 200 nm of Pt coating on 250 μ m thick Ti felt. The objective of this study is to reduce the commercial PTL costs without affecting its performance in PEMWE operating conditions. As per January 2025, the cost of Pt is 30,218.49 USD/kg [56] whereas the cost of Nb is 77.64 USD/kg [30]. Therefore, in the case of A4-ml, the coated Pt is reduced from 200 nm to 50 nm, achieving a significant reduction in coating costs. Subsequently, to evaluate its performance, A4-ml is compared with A5-cmc under in-situ condition of PEMWE. Fig. 11a shows the cell performance of both samples. At 2.0 A/cm², A4-ml (2.050 V) shows similar performances as A5-cmc (2.044 V) due to the presence of Pt top layer in both cases. However, to distinguish the effects of ohmic, kinetic and mass transport overpotential, IR free voltage is plotted (Fig. 11a). The protocol to calculate all three overpotentials [57] is provided in section S-1 of the Supplementary Information. At 2.0 A/cm², IR free voltage (Fig. 11a) for A4-ml and A5-cmc are 1.599 V and 1.603 V, respectively, indicating higher voltage drop (0.451 V) for the former compared to latter (0.441 V). This observation is in line with the ohmic overpotential (η_{ohmic}) data of both PTLs. Fig. 11b shows that below 0.5 A/cm², A4-ml and A5-cmc exhibit similar η_{ohmic} , which begin to diverge at high current densities. The reason being the difference in High frequency resistance (HFR) (Figure S9 in Supplementary Information) between two samples. Note that although the differences in HFR seems nominal, their impact on η_{ohmic} is greater at high current densities ($\eta_{ohmic} = I \times HFR$), resulting in a higher voltage drop in A4-ml compared to A5-cmc, as mentioned above.

Furthermore, the lower values of HFR in A5-cmc compared to A4-ml, is consistent with ex-situ ICR measurement (as discussed in Section 3.3). The underlying cause of this trend is explained hereafter. The ohmic overpotential, usually is a combination of bulk resistance of each component as well as resistance originating from their interfacial contacts. Since all the components in A4-ml and A5-cmc are identical except the PTL coatings, the difference in ohmic resistance could only arise due to the ICR difference between PTL and MEA. Note that despite having same trend, ICR values are different in both ex-situ and in-situ measurements. This is due to the difference in the temperature, current density, materials, pressure etc. between the two situations [11].

Next, A4-ml shows (Fig. 11b) marginally lower kinetic and mass transport overpotential than A5-cmc. This observation seems strange as both A4-ml and A5-cmc contains Pt top layer, which ought to produce similar kinetics and mass transport loss. The origin of this behavior is unclear but could be attributed to higher toughness of multi-layered coatings than single layered coatings [26]. PTLs are subjected to compressive stress during the components integration inside the PEMWE stack, which could lead to slight deformation or microcracks formations in A5-cmc's top layer, resulting in exposure of the titanium substrate. This may further lead to lower OER (kinetic loss) and entrapment of gases (mass transport loss). Hence, coatings must exhibit high hardness (ability to resist deformation) and toughness (ability to resist fracture) inside the stack. The combined effect of hard (Nb) and soft (Pt) layers causes dislocations pile up at the interface, which in turn gives rise to strain hardening in the coated samples [27]. Moreover, any cracks generation in Pt top layer gets deflected at the interface and its propagation ceases [26,28]. Thus, energy absorption ability of the coatings increases in A4-ml, resulting in high toughness of the coating.

To put it briefly, despite having thinner Pt layer (50 nm), multi-layered NbPt sample (A4-ml) performs on par with single layered commercial sample (A5-cmc) under in-situ operating conditions. However, due to its higher ohmic overpotential compared to A5-cmc, A4-ml shows slightly lower cell performance at higher current densities. This calls for a future work, to bring down the ICR in the case of A4-ml. Nevertheless, the present work created an opportunity for utilization and optimization of Nb as an interlayer on the PTL for application in PEM water electrolyzer.

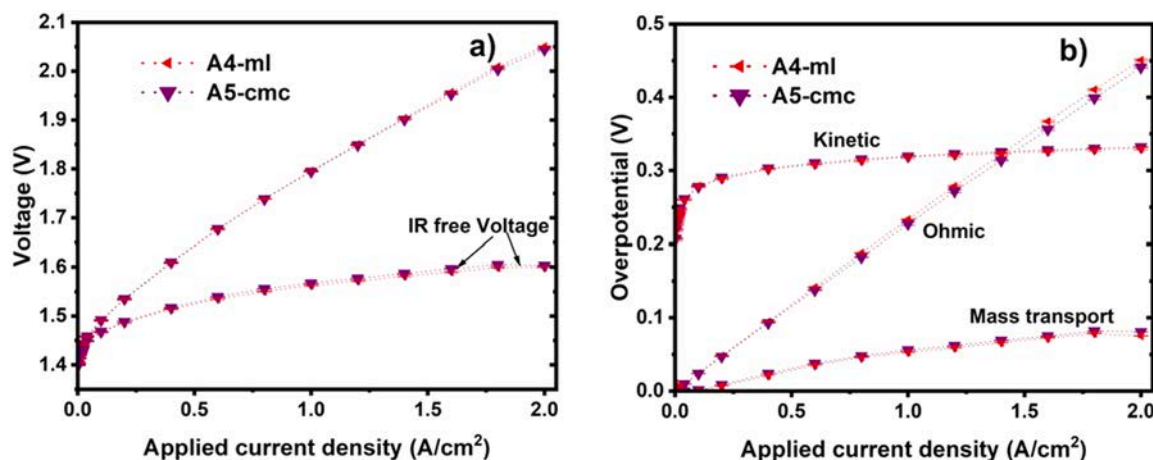


Fig. 11. (a) Polarization curve depicting the cell and IR free voltage of A4-ml and A5-cmc (b) Contribution of kinetic, ohmic and mass transport overpotentials for A4-ml and A5-cmc samples inside PEMWE stack. The error bars depict the individual standard deviation corresponding to each value.

4. Conclusions

Due to harsh acidic conditions and high operational voltages, PEMWE cell components like BPPs and PTLs are coated with expensive Pt coatings to ensure corrosion protection and high electrical conductivity. Therefore, Nb was introduced as an interlayer between the Pt and Ti PTL to reduce coating costs without compromising cell performance. The results showed that:

- Nb solely cannot be utilized as a top layer for corrosion protection of PTL, hence Pt top layer is mandatory to reduce the overall ICR. Post-corrosion morphology analysis showed an excellent adhesion of Nb with both Ti substrate and Pt top layer. Moreover, multilayered NbPt coating exhibited higher durability (102 h) than the co-deposited counterpart (17 h) due to the poor adhesion of Pt with Nb₂O₅ and greater residual strain in the latter.
- Compared to commercial PTL, the multi-layered NbPt coated PTL exhibited superior corrosion resistance, comparable ICR, and a longer simulated durability. This was attributed to better Ti-Nb-Pt adhesion, lower Pt oxidation, reduced galvanic effect and higher contact angle in case of A4-ml. Under in-situ testing, multi-layered sample A4-ml (2.050 V) showed similar performance to commercial sample A5-cmc (2.044 V) at 2.0 A/cm². These results demonstrate the prospects of multi-layered NbPt coating (Nb=350 nm and Pt=50 nm) on the Ti PTL to be used as an alternative to single layered commercial PTL (Pt = 200 nm).

Nomenclature

E_{corr} , corrosion potential, V
 I_{corr} , corrosion current density, $\mu\text{A}/\text{cm}^2$
 β_a, β_c , tafel slopes, mV/decade
 R_p , polarization resistance, $\Omega\cdot\text{cm}^2$
 I_{pass} , passivation current density, mA/cm^2
 η_{ohmic} , ohmic overpotential, V
 HFR , high frequency resistance, $\Omega\cdot\text{cm}^2$

Abbreviations

PTLs, porous transport layers
 PEMWE, proton exchange membrane water electrolyzer
 GHG, greenhouse gases
 MEA, membrane electrode assembly
 PGMs, pt-group metals
 ICR, interfacial contact resistance

FIB, focused ion beam
 OCP, open circuit potential
 CA, chronoamperometry
 EOL, end of life
 SEM, scanning electron microscopy
 EDS, energy dispersive x-ray spectroscopy
 XPS, x-ray photoelectron spectroscopy
 GDLs, gas diffusion layers
 EIS, electrochemical impedance spectroscopy
 BSE, backscattered electron
 OER, oxygen evolution reaction

CRediT authorship contribution statement

Anurag: Writing – original draft, Visualization, Validation, Methodology, Investigation, Formal analysis, Conceptualization. **Abhay Gupta:** Writing – review & editing, Visualization, Methodology. **Samaneh Shahgaldi:** Writing – review & editing, Supervision, Resources, Project administration, Methodology, Funding acquisition, Conceptualization.

Declaration of competing interest

The authors declare that they have no known competing financial interests or personal relationships that could have appeared to influence the work reported in this paper.

Acknowledgements

Shahgaldi research team at the Hydrogen Research Institute, University of Quebec a Trois Rivières would like to acknowledge the support of the Natural Sciences and Engineering Research Council of Canada (NSERC), Canada Research Chair (CRC-2019–00354), Discovery grant (CRSNG-DGECR-2022–00058), Prima Quebec (R23–13–005), NSERC-Alliance (3289542) and Mitacs Accelerate (IT30506). The authors would like to thank Niobay team for their constant support.

Supplementary materials

Supplementary material associated with this article can be found, in the online version, at [doi:10.1016/j.electacta.2025.147053](https://doi.org/10.1016/j.electacta.2025.147053).

Data availability

Data will be made available on request.

References

- [1] Net Zero Coalition | United Nations, (n.d.). <https://www.un.org/en/climatechange/net-zero-coalition> (accessed December 20, 2024).
- [2] Causes and effects of climate change | United Nations, (n.d.). <https://www.un.org/en/climatechange/science/causes-effects-climate-change> (accessed December 20, 2024).
- [3] M.A. Habib, G.A.Q. Abdulrahman, A.B.S. Alqaity, N.A.A. Qasem, Hydrogen combustion, production, and applications: a review, *Alex Eng. J.* 100 (2024) 182–207, <https://doi.org/10.1016/J.AEJ.2024.05.030>.
- [4] A. Ajanovic, M. Sayer, R. Haas, The economics and the environmental benignity of different colors of hydrogen, *Int. J. Hydrog. Energy* 47 (2022) 24136–24154, <https://doi.org/10.1016/J.IJHYDENE.2022.02.094>.
- [5] K. Zhang, X. Liang, L. Wang, K. Sun, Y. Wang, Z. Xie, Q. Wu, X. Bai, M.S. Hamdy, H. Chen, X. Zou, Status and perspectives of key materials for PEM electrolyzer, *Nano Res. Energy* 1 (2022), <https://doi.org/10.26599/NRE.2022.9120032> e9120032–e9120032.
- [6] T.L. Doan, H.E. Lee, S.S.H. Shah, M.J. Kim, C.H. Kim, H.S. Cho, T. Kim, A review of the porous transport layer in polymer electrolyte membrane water electrolysis, *Int. J. Energy Res.* 45 (2021) 14207–14220, <https://doi.org/10.1002/ER.6739>.
- [7] J. Parra-Restrepo, R. Bligny, J. Dillet, S. Didierjean, D. Stemmelen, C. Moyné, A. Degiovanni, G. Maranzana, Influence of the porous transport layer properties on the mass and charge transfer in a segmented PEM electrolyzer, *Int. J. Hydrog. Energy* 45 (2020) 8094–8106, <https://doi.org/10.1016/J.IJHYDENE.2020.01.100>.
- [8] F. Arbabi, A. Kalantarian, R. Abouattallah, R. Wang, J.S. Wallace, A. Bazyalak, Feasibility study of using microfluidic platforms for visualizing bubble flows in electrolyzer gas diffusion layers, *J. Power. Sources.* 258 (2014) 142–149, <https://doi.org/10.1016/J.JPOWSOUR.2014.02.042>.
- [9] E. Leonard, A.D. Shum, S. Normile, D.C. Sabarirajan, D.G. Yared, X. Xiao, I. V. Zenyuk, Operando X-ray tomography and sub-second radiography for characterizing transport in polymer electrolyte membrane electrolyzer, *Electrochim. Acta* 276 (2018) 424–433, <https://doi.org/10.1016/J.ELECTACTA.2018.04.144>.
- [10] C. Liu, K. Wippermann, M. Rasinski, Y. Suo, M. Shviro, M. Carmo, W. Lehnert, Constructing a multifunctional interface between membrane and porous transport layer for water electrolyzers, *ACS. Appl. Mater. Interfaces.* 13 (2021) 16182–16196, <https://doi.org/10.1021/acsami.0c20690>.
- [11] C. Rakousky, U. Reimer, K. Wippermann, M. Carmo, W. Lueke, D. Stolten, An analysis of degradation phenomena in polymer electrolyte membrane water electrolysis, *J. Power. Sources.* 326 (2016) 120–128, <https://doi.org/10.1016/j.jpowsour.2016.06.082>.
- [12] C. Liu, M. Shviro, A.S. Gago, S.F. Zaccarini, G. Bender, P. Gazdzicki, T. Morawietz, I. Biswas, M. Rasinski, A. Everwand, R. Schierholz, J. Pfeilsticker, M. Müller, P. P. Lopes, R.A. Eichel, B. Pivovar, S. Pylypenko, K.A. Friedrich, W. Lehnert, M. Carmo, Exploring the interface of skin-layered titanium fibers for electrochemical water splitting, *Adv. Energy Mater.* 11 (2021) 2002926, <https://doi.org/10.1002/AENM.202002926>.
- [13] S. Stiber, H. Balzer, A. Wierhake, F.J. Wirkert, J. Roth, U. Rost, M. Brodmann, J. K. Lee, A. Bazyalak, W. Waiblinger, A.S. Gago, K.A. Friedrich, Porous transport layers for proton exchange membrane electrolysis under extreme conditions of current density, temperature, and pressure, *Adv. Energy Mater.* 11 (2021), <https://doi.org/10.1002/aenm.202100630>.
- [14] H. Ye, L. Chen, D. Shen, S. Li, Z. Tu, Performance of Ta/TaN coated titanium felt for proton exchange membrane water electrolysis, *Int. J. Hydrog. Energy* 93 (2024) 1022–1030, <https://doi.org/10.1016/J.IJHYDENE.2024.11.057>.
- [15] H. Ye, Z. Tu, S. Li, Electrochemical performance of metal nitride coated titanium bipolar plate for proton exchange membrane water electrolyser, *J. Power. Sources.* 595 (2024), <https://doi.org/10.1016/j.jpowsour.2024.234052>.
- [16] Q. Meng, X. Yue, L. Shang, X. Liu, F. Wang, G. Zhang, Corrosion behavior of metallic coatings on titanium bipolar plates of proton exchange membrane water electrolysis, *Int. J. Hydrog. Energy* 63 (2024) 1105–1115, <https://doi.org/10.1016/J.IJHYDENE.2024.03.242>.
- [17] S. Stiber, M. Hehemann, M. Carmo, M. Müller, K.E. Ayers, C. Capuano, N. Danilovic, T. Morawietz, I. Biswas, P. Gazdzicki, J.F. Heger, A.S. Gago, K. A. Friedrich, Long-term operation of Nb-coated stainless steel bipolar plates for proton exchange membrane water electrolyzers, *Adv. Energy Sustain Res.* 3 (2022) 2200024, <https://doi.org/10.1002/AESR.202200024>.
- [18] L.H. Prado, S. Virtanen, N. Weineck, A. Ghicov, F. Kessler, How to perform corrosion experiments for proton exchange membrane water electrolysis bipolar plates, *J. Power. Sources.* 613 (2024) 234815, <https://doi.org/10.1016/J.JPOWSOUR.2024.234815>.
- [19] Y. Abe, M. Kawamura, K. Sasaki, Preparation of PtO and α -PtO₂ thin films by reactive sputtering and their electrical properties, *Jpn. J. Appl. Phys.* 38 (1999) 2092–2096, <https://doi.org/10.1143/JJAP.38.2092>.
- [20] A. Yildiz, S.B. Lisesivdin, M. Kasap, D. Mardare, Electrical properties of TiO₂ thin films, *J. Non. Cryst. Solids.* 354 (2008) 4944–4947, <https://doi.org/10.1016/j.jnoncrsol.2008.07.009>.
- [21] C. Nico, T. Monteiro, M.P.F. Graça, Niobium oxides and niobates physical properties: review and prospects, *Prog. Mater. Sci.* 80 (2016) 1–37, <https://doi.org/10.1016/j.pmatsci.2016.02.001>.
- [22] K. Bao, J. Meng, J.D. Poplawsky, M. Skowronski, Electrical conductivity of TaOx as function of composition and temperature, *J. Non. Cryst. Solids.* 617 (2023) 122495, <https://doi.org/10.1016/J.JNONCRYSOL.2023.122495>.
- [23] J.M. Lackner, L. Major, M. Kot, Microscale interpretation of tribological phenomena in Ti/TiN soft-hard multilayer coatings on soft austenite steel substrates, *Bull Pol Acad Sci: Tech Sci* 59 (2011) 343–356, <https://doi.org/10.2478/V10175-011-0042-X>.
- [24] D. Zhou, H. Peng, L. Zhu, H. Guo, S. Gong, Microstructure, hardness and corrosion behaviour of Ti/TiN multilayer coatings produced by plasma activated EB-PVD, *Surf. Coat. Technol.* 258 (2014) 102–107, <https://doi.org/10.1016/J.SURFcoat.2014.09.058>.
- [25] L.A. Dobrzański, K. Lukaszewicz, A. Kriz, Properties of the multi-layer Ti/CrN and Ti/TiAlN coatings deposited with the PVD technique onto the brass substrate, *J. Mater. Process. Technol.* 143–144 (2003) 832–837, [https://doi.org/10.1016/S0924-0136\(03\)00351-0](https://doi.org/10.1016/S0924-0136(03)00351-0).
- [26] H. Holleck, M. Lahres, P. Woll, Multilayer coatings—Influence of fabrication parameters on constitution and properties, *Surf. Coat. Technol.* 41 (1990) 179–190, [https://doi.org/10.1016/0257-8972\(90\)90166-A](https://doi.org/10.1016/0257-8972(90)90166-A).
- [27] S.J. Bull, A.M. Jones, Multilayer coatings for improved performance, *Surf. Coat. Technol.* 78 (1996) 173–184, [https://doi.org/10.1016/0257-8972\(94\)02407-3](https://doi.org/10.1016/0257-8972(94)02407-3).
- [28] Ming Yuan He, A.G. Evans, J.W. Hutchinson, Crack deflection at an interface between dissimilar elastic materials: role of residual stresses, *Int. J. Solids. Struct.* 31 (1994) 3443–3455, [https://doi.org/10.1016/0020-7683\(94\)90025-6](https://doi.org/10.1016/0020-7683(94)90025-6).
- [29] S. Lædre, O.E. Kongstein, A. Oedegaard, H. Karoliusen, F. Seland, Materials for Proton Exchange membrane water electrolyzer bipolar plates, *Int J Hydrog Energy* 42 (2017) 2713–2723, <https://doi.org/10.1016/J.IJHYDENE.2016.11.106>.
- [30] Daily Niobium /Tantalum price, Lme Comex Shfe Price Niobium / Tantalum live | SMM - Met Mark (January 15, 2025) n.d, <https://www.metal.com/Niobium-Tantalum>. accessed.
- [31] Current Tantalum Price, Historical prices, USA, China, Europe, Asia, Australia prices, (n.d.). <https://www.scrapmonster.com/metal-prices/minor-metals/tantalum/798> (accessed January 25, 2025).
- [32] E. Asselin, T.M. Ahmed, A. Alfantazi, Corrosion of niobium in sulphuric and hydrochloric acid solutions at 75 and 95°C, *Corros. Sci.* 49 (2007) 694–710, <https://doi.org/10.1016/J.CORSCI.2006.05.028>.
- [33] E. Kuhnert, M. Heidinger, A. Bernroither, Ö. Kiziltan, E. Berger, V. Hacker, M. Bodner, Fluoride emission rate analysis in proton exchange membrane water electrolyzer cells, *Front. Energy Res.* 12 (2024) 1457310, <https://doi.org/10.3389/FENRG.2024.1457310/BIBTEX>.
- [34] Y. Li, J. Xu, Is niobium more corrosion-resistant than commercially pure titanium in fluoride-containing artificial saliva? *Electrochim. Acta* 233 (2017) 151–166, <https://doi.org/10.1016/J.ELECTACTA.2017.03.015>.
- [35] P. Lettenmeier, R. Wang, R. Abouattallah, B. Saruhan, O. Freitag, P. Gazdzicki, T. Morawietz, R. Hiesgen, A.S. Gago, K.A. Friedrich, Low-cost and durable bipolar plates for proton exchange membrane electrolyzers, *Sci. Rep.* 7 (2017), <https://doi.org/10.1038/srep44035>.
- [36] H. Kalhori, M. Johar, L. Moradizadeh, S. Shahgaldi, H. Kalhori, M. Johar, L. Moradizadeh, S. Shahgaldi, Niobium interlayer coating: Is it a practical approach to tune the protective Pt loading in PEM water electrolyzers? *ECSTr* 114 (2024) 499–513, <https://doi.org/10.1149/1.1405.0499ECSTr>.
- [37] K. Lin, X. Li, L. Tian, H. Dong, Active screen plasma surface co-alloying of 316 austenitic stainless steel with both nitrogen and niobium for the application of bipolar plates in proton exchange membrane fuel cells, *Int. J. Hydrog. Energy* 40 (2015) 10281–10292, <https://doi.org/10.1016/J.IJHYDENE.2015.06.010>.
- [38] A.V. Ingle, V.S. Raja, J. Rangarajan, P. Mishra, Corrosion resistant quaternary Al–Cr–Mo–N coating on type 316L stainless steel bipolar plates for proton exchange membrane fuel cells, *Int. J. Hydrog Energy* 45 (2020) 3094–3107, <https://doi.org/10.1016/J.IJHYDENE.2019.11.119>.
- [39] L. Moradizadeh, P.V. Madhavan, Y.M. Chellehbari, A. Gupta, X. Li, S. Shahgaldi, Porous transport layers with low Pt loading having Nb–Ta alloy as interlayer for proton exchange membrane water electrolyzers, *Int. J. Hydrog. Energy* 94 (2024) 1114–1129, <https://doi.org/10.1016/J.IJHYDENE.2024.11.192>.
- [40] M. Johar, L. Moradizadeh, A. Gupta, Y. Mehdizadeh Chellehbari, X. Li, S. Shahgaldi, Development of novel Nb and Ta multilayer coatings for corrosion protection of Ti-based bipolar plates for proton exchange membrane fuel cells, *Corros. Sci.* 245 (2025) 112707, <https://doi.org/10.1016/J.CORSCI.2025.112707>.
- [41] H. Wang, M.A. Sweikart, J.A. Turner, Stainless steel as bipolar plate material for polymer electrolyte membrane fuel cells, *J. Power. Sources.* 115 (2003) 243–251, [https://doi.org/10.1016/S0378-7753\(03\)00023-5](https://doi.org/10.1016/S0378-7753(03)00023-5).
- [42] R. Ghamsarizadeh, B. Ramezanzadeh, H.E. Mohammadloo, Corrosion measurements in coatings and paintings, electrochemical and analytical techniques for sustainable Corrosion monitoring: advances, challenges and opportunities (2023) 217–264, <https://doi.org/10.1016/B978-0-443-15783-7.00008-6>.
- [43] D.R. Do Carmo, C.A. Picone, Corrosion resistance of niobium, tantalum and titanium in sea WATER and sulfuric ACID, in: ECS Meeting Abstracts, 2013, p. 1722, <https://doi.org/10.1149/MA2013-02/17/1722>. MA2013-02.
- [44] I. Kondo, T. Yoneyama, O. Takenaka, A. Kinbara, Formation of high adhesive and pure Pt layers on TiO₂, *J. Vac. Sci. Technol. A: Vac. Surf. Films* 10 (1992) 3456–3459, <https://doi.org/10.1116/1.577802>.
- [45] R.C. Budhani, S. Prakash, H.J. Doerr, R.F. Bunshah, Summary abstract: oxygen enhanced adhesion of platinum films deposited on thermally grown alumina surfaces, *J Vac Sci. Technol. A: Vac. Surf. Films* 4 (1986) 3023–3024, <https://doi.org/10.1116/1.573619>.
- [46] H.P. Lim, W.Y.H. Liew, G.J.H. Melvin, Z.T. Jiang, A short review on the phase structures, oxidation kinetics, and mechanical properties of complex Ti–Al alloys, *Mater (Basel)* 14 (2021) 1677, <https://doi.org/10.3390/MA14071677>, 2021Page 1677 14.
- [47] X. Wang, H. Luo, H. Cheng, L. Yue, Z. Deng, J. Yao, X. Li, Investigation on the performance of Pt surface modified Ti bipolar plates in proton exchange membrane water electrolyzer, *Appl. Energy* 357 (2024), <https://doi.org/10.1016/j.apenergy.2023.122517>.

- [48] A. Nigro, G. Nobile, M.G. Rubino, R. Vaglio, Electrical resistivity of polycrystalline niobium nitride films, *Phys. Rev. B* 37 (1988) 3970–3972, <https://doi.org/10.1103/PHYSREVB.37.3970>.
- [49] A. Kellenberger, D. Duca, N. Vaszilcsin, C.M. Craciunescu, Electrochemical evaluation of niobium corrosion resistance in simulated anodic PEM electrolyzer environment, *Int. J. Electrochem. Sci.* 15 (2020) 10664–10673, <https://doi.org/10.20964/2020.11.47>.
- [50] C. Gaona-Tiburcio, M. Montoya-Rangel, J.A. Cabral-Miramontes, F. Estupiñán-López, P. Zambrano-Robledo, R.O. Cruz, J.G. Chacón-Nava, M.Á. Baltazar-Zamora, F. Almeraya-Calderón, Corrosion resistance of multilayer coatings deposited by PVD on Inconel 718 using electrochemical impedance spectroscopy technique, *coatings* 2020, Vol. 10, Page 521 10 (2020) 521. <https://doi.org/10.3390/COATINGS10060521>.
- [51] D.M. Marulanda, J.J. Olaya, U. Piratoba, A. Mariño, E. Camps, The effect of bilayer period and degree of unbalancing on magnetron sputtered Cr/CrN nano-multilayer wear and corrosion, *Thin. Solid. Films.* 519 (2011) 1886–1893, <https://doi.org/10.1016/j.TSE.2010.10.010>.
- [52] H.W. Chang, Y.C. Tsai, C.W. Cheng, C.Y. Lin, P.H. Wu, Preparation of platinum/carbon nanotube in aqueous solution by femtosecond laser for non-enzymatic glucose determination, *Sens. Actuators. B Chem.* 183 (2013) 34–39, <https://doi.org/10.1016/j.SNB.2013.03.115>.
- [53] H.J. Chun, D.B. Kim, D.H. Lim, W.D. Lee, H.I. Lee, A synthesis of CO-tolerant Nb₂O₅-promoted Pt/C catalyst for direct methanol fuel cell; its physical and electrochemical characterization, *Renew. Energy* 35 (2010) 6399–6408, <https://doi.org/10.1016/j.ijhydene.2010.03.061>.
- [54] J.S. Hammond, N. Winograd, XPS spectroscopic study of potentiostatic and galvanostatic oxidation of Pt electrodes in H₂SO₄ and HClO₄, *J. Electroanal. Chem. Interfacial. Electrochem.* 78 (1977) 55–69, [https://doi.org/10.1016/S0022-0728\(77\)80422-1](https://doi.org/10.1016/S0022-0728(77)80422-1).
- [55] K.S. Kim, N. Winograd, R.E. Davis, Electron spectroscopy of platinum-oxygen surfaces and application to electrochemical studies, *J. Am. Chem. Soc.* 93 (1971) 6296–6297, https://doi.org/10.1021/JA00752A065/ASSET/JA00752A065.FP.PNG_V03.
- [56] Platinum price in USD per kilogram for today, (n.d.). [https://www.bullionbypost.eu/platinum-price/today/kilograms/USD/\(accessed January 15, 2025\)](https://www.bullionbypost.eu/platinum-price/today/kilograms/USD/(accessed January 15, 2025)).
- [57] M. Suermann, T.J. Schmidt, F.N. Büchi, Cell performance determining parameters in high pressure water electrolysis, *Electrochim. Acta* 211 (2016) 989–997, <https://doi.org/10.1016/J.ELECTACTA.2016.06.120>.